How to cite: *Angew. Chem. Int. Ed.* **2021**, *60*, 2078–2083
International Edition: doi.org/10.1002/anie.202012089
German Edition: doi.org/10.1002/ange.202012089

Photobioelectrochemistry

A Tandem Solar Biofuel Cell: Harnessing Energy from Light and Biofuels

Marc Riedel, Soraya Höfs, Adrian Ruff, Wolfgang Schuhmann, and Fred Lisdat**

Abstract: *We report on a photobioelectrochemical fuel cell consisting of a glucose-oxidase-modified $BiFeO_3$ photobiocathode and a quantum-dot-sensitized inverse opal TiO_2 photobioanode linked to FAD glucose dehydrogenase via a redox polymer. Both photobioelectrodes are driven by enzymatic glucose conversion. Whereas the photobioanode can collect electrons from sugar oxidation at rather low potential, the photobiocathode shows reduction currents at rather high potential. The electrodes can be arranged in a sandwich-like manner due to the semi-transparent nature of $BiFeO_3$, which also guarantees a simultaneous excitation of the photobioanode when illuminated via the cathode side. This tandem cell can generate electricity under illumination and in the presence of glucose and provides an exceptionally high OCV of about 1 V. The developed semi-artificial system has significant implications for the integration of biocatalysts in photoactive entities for bioenergetic purposes, and it opens up a new path toward generation of electricity from sunlight and (bio)fuels.*

Interfacing biotic components with abiotic entities on electrodes has gained considerable interest for power generation, the production of fuels and chemicals, but also for sensing.[1,2] Particularly, the coupling of photoactive materials with biocatalysts provides a promising strategy for the introduction of new catalytic features in solar-driven signal chains, which are not feasible by each component alone.[3]

Besides the connection of the photoactive entity to the electrode, in particular, the efficient linkage of the enzyme is a key for the construction of high performance photoactive biohybrids. Often light-driven signal chains are established via photoelectrochemical oxidation/reduction of enzymatic products and substrates,[4–7] or mediators,[8–11] while the direct electron transfer remains challenging.[12,13] Recently, we and others have demonstrated that FAD glucose dehydrogenase[14] and photosystem II[15–17] can be wired to photoanodes, resulting in an improved onset potential for glucose and H_2O oxidation, respectively. If such a biohybrid photoanode is coupled to a light insensitive biocathode, electrons from biocatalytic oxidation can be transferred to a reductase reaction under illumination for the generation of electric energy with a high operational voltage,[17] or the production of hydrogen[15] and formate.[16] Several photobiocathodes have been reported in literature, however, they often suffer from rather high overpotentials to generate a photocurrent or to drive an enzymatic reaction.[18,19] Moreover, (photo-)cathodes that mimic enzymatic reactions such as H^+, H_2O_2 or O_2 reduction are often significantly worse in terms of overpotential and conversion rate than their biocatalytic counterparts. For example, bioelectrocatalytic H_2O_2 reduction using horseradish peroxidase[20,21] and decaheme cytochrome[22] is found to occur several hundred mVs more positive than in most photoelectrocatalytic approaches.[19,23,24] Therefore, new strategies for the construction of photo(bio)cathodes are necessary to overcome energetic losses for light-driven chemical reduction.

Besides the use of single photoactive electrodes, the combination photocathodes with photoanodes in a solar tandem cell format has become a focus of research aiming to improve solar yield and operating voltage.[25] Construction of a solar tandem cell with two photobioelectrodes could set new benchmarks for the synthesis of chemicals, but can also provide a new way for the construction of photobiofuel cells, which combine energy production from light and (bio)fuels.

Here, we introduce a new concept for the generation of power from light and biofuels by combination of a glucose converting photobiocathode with a glucose-powered photobioanode (Scheme 1). For this, a $BiFeO_3$ photocathode with high photocatalytic activity towards H_2O_2 reduction has been coupled to glucose oxidase (GOx). The biocatalytic glucose turnover generates H_2O_2, which accepts excited electrons from the photocathode under concomitant amplification of the cathodic photocurrent. The final $BiFeO_3|GOx$ photobiocathode is coupled to a glucose converting photobioanode in a photobioelectrochemical tandem cell (PBTC) set-up, enabling the generation of energy with high cell voltages under illumination and in the presence of biofuel.

As a starting point we have investigated $BiFeO_3$ for its suitability as new semi-transparent, light-sensitive photobio-

[*] Dr. M. Riedel, S. Höfs, Prof. Dr. F. Lisdat
Biosystems Technology, Institute of Life Sciences and Biomedical Technologies, Technical University of Applied Sciences Wildau
Hochschulring 1, 15745 Wildau (Germany)
E-mail: riedel@th-wildau.de
flisdat@th-wildau.de
Dr. A. Ruff, Prof. Dr. W. Schuhmann
Analytical Chemistry—Center for Electrochemical Sciences (CES)
Faculty of Chemistry and Biochemistry, Ruhr-University Bochum
Universitätstr. 150, 44780 Bochum (Germany)
Dr. A. Ruff
PPG (Deutschland) Business Support GmbH, EMEA Packaging Coatings
Erlenbrunnenstr. 20, 72411 Bodelshausen (Germany)
Supporting information and the ORCID identification number(s) for the author(s) of this article can be found under: https://doi.org/10.1002/anie.202012089.

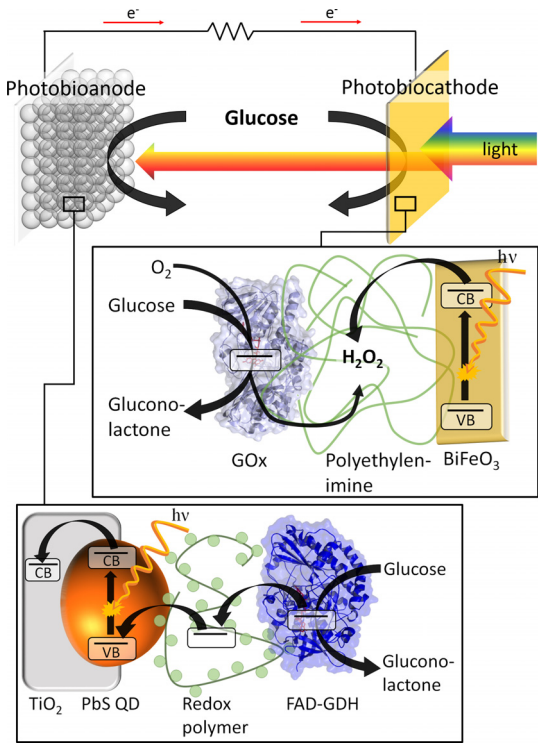

Scheme 1. Illustration of the photobioelectrochemical tandem cell consisting of a $BiFeO_3$ | GOx photobiocathode and an IO-TiO_2 | PbS-| P_{Os} | FAD-GDH photobioanode, and the proposed electron transfer steps of the signal chain under illumination and in the presence of glucose. PBD ID GOx: 1CF3,[30] PDB ID FAD-GDH: 4YNT.[31]

cathode material due to its photoelectrochemical properties.[26,27] $BiFeO_3$ photocathodes have been prepared on fluorine doped tin oxide (FTO) slides by a spin coating approach using $Bi(NO_3)_3$ and $Fe(NO_3)_3$ with a ratio of 1:1 and subsequent sintering. The resulting $BiFeO_3$ layer is yellowish colored and from the UV/Vis data an optical band gap of about 2.7 eV can be determined—in good agreement with a previous report (Supporting Information, Figures S1 and S2).[28,29] SEM images reveal the formation of a rather homogeneous porous surface with no large agglomerates (Figure 1 A), preventing larger light scattering effects and thus providing enough transparency (about 65 % at 550 nm) to allow excitation of a photobioanode with a smaller band gap (i.e. larger wavelength excitation range).

Photocatalytic H_2O_2 reduction is often counterbalanced by disturbing H_2O_2 oxidation processes occurring at the base electrode, thus reducing the performance in terms of potential behavior. To study this effect basic electrochemical investigations have been performed in the dark with pure FTO and FTO | $BiFeO_3$ electrodes in the presence and absence of H_2O_2. While pure FTO electrodes show strong H_2O_2 oxidation starting at ≈0.3 V vs. Ag/AgCl (1 M KCl), anodic processes can drastically be reduced by modification with $BiFeO_3$ (Figure 1 A). This indicates that $BiFeO_3$ passivates the FTO and interferes with the penetration of H_2O_2 to the underlying FTO and considerably minimize parasitic H_2O_2 oxidation. This surface passivation effect has also been verified by impedance experiments in the presence of ferri/ferrocyanide,

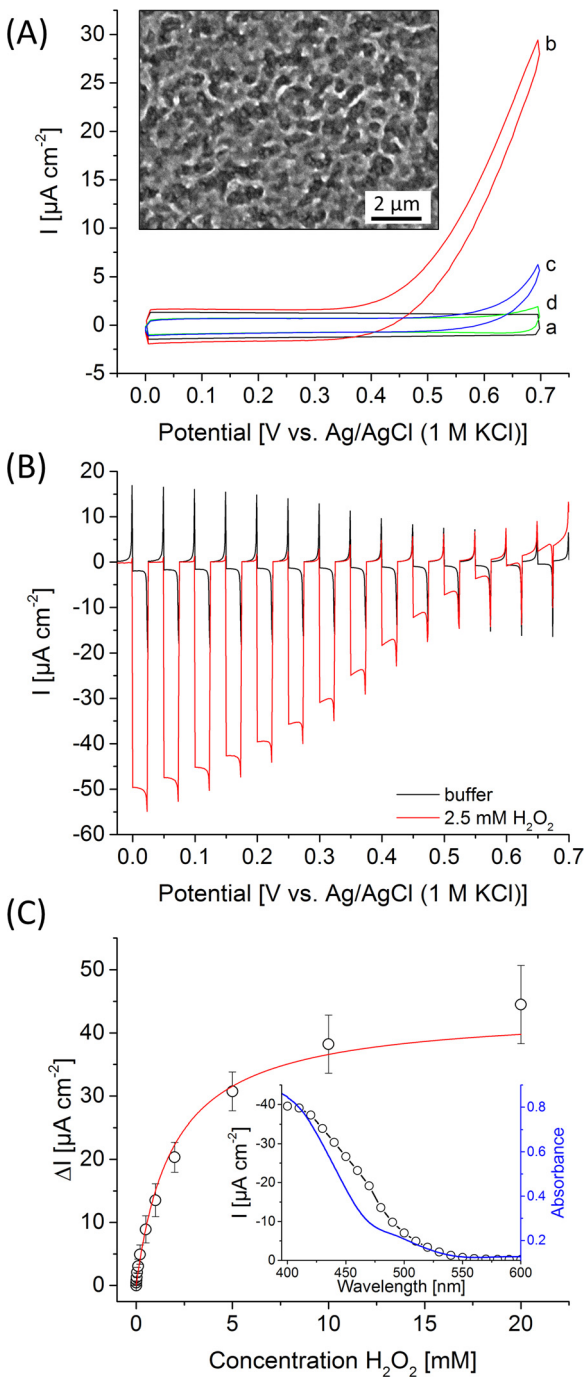

Figure 1. A) Cyclic voltammograms of pure FTO slides (a,b) and FTO | $BiFeO_3$ electrodes (c,d) in the presence (b,c) and absence (a,d) of 2.5 mM H_2O_2 in the dark (100 mVs^{-1}). Inset: SEM image of a $BiFeO_3$ electrode with a 10000-fold magnification. B) Chopped-light voltammetry of a $BiFeO_3$ electrode in the presence and absence of 2.5 mM H_2O_2 (100 $mWcm^{-2}$; 10 mVs^{-1}). C) Photocurrent density change ΔI of a $BiFeO_3$ electrode before and after addition of different H_2O_2 concentrations (100 $mWcm^{-2}$; 0.2 V vs. Ag/AgCl, 1 M KCl). Inset: wavelength-dependent photocurrent response (black points) and UV/Vis spectrum (blue line) of a $BiFeO_3$ electrode (0.2 V vs. Ag/AgCl, 1 M KCl).

resulting in a 40-fold enhancement of the charge transfer resistance from 20 kΩ for FTO to about 800 kΩ for $BiFeO_3$ electrodes (Figure S3).

The $BiFeO_3$ electrode has been first investigated photoelectrochemically via chopped light voltammetry. Figure 1B displays the formation of a cathodic photocurrent over the whole investigated potential range in buffer. In the presence of H_2O_2 this reduction current is significantly enhanced. For instance, at 0 V vs. Ag/AgCl (1 M KCl) the current is amplified 15 times ($-2.8 \pm 1.9\ \mu A\,cm^{-2}$ to $-42.3 \pm 8.7\ \mu A\,cm^{-2}$), giving rise to an external quantum efficiency (EQE) of $0.1 \pm 0.02\,\%$. In contrast, pure FTO slides exhibit no photoelectrochemical response (Figure S4). An onset potential of 0.63 ± 0.016 V has been obtained for H_2O_2 reduction, which is to the best of our knowledge more than 0.2 V more positive than previous PEC approaches[19,23,24] and also slightly exceeds the onset potential of light-independent bioelectrocatalytic approaches using enzymes.[20–22] This highlights the outstanding photoelectrocatalytic activity found for the $BiFeO_3$ electrodes as peroxidase mimics. Moreover, wavelength resolved measurements demonstrate that the photocurrent response of the $BiFeO_3$ nicely matches with the absorbance features of the structures, showing reasonable photocurrents below 550 nm and proves $BiFeO_3$ as the origin of the photosignal (Figure 1C).

The $BiFeO_3$ photocathodes show a typical saturation-type concentration behavior for H_2O_2 reduction giving first signals at 5 μM up to concentrations of 20 mM H_2O_2 at a rather positive working potential of 0.2 V vs. Ag/AgCl (1 M KCl) (Figure 1C; Figure S5). This makes $BiFeO_3$ photocathodes interesting candidates for sensing and for the combination with H_2O_2 producing enzymes. Furthermore, a reasonable stability of about 80 % of the initial signal has been found for the light-directed H_2O_2 reduction after 15 min pulsed illumination (Figure S6).

Based on these findings, we have combined the photocatalytic activity of the $BiFeO_3$ electrode towards H_2O_2 with the biocatalytic features of GOx for the construction of a glucose-driven photobiocathode. The signal chain is initiated by the biocatalytic turnover of glucose to gluconic acid and concomitant generation of H_2O_2, which reacts at the $BiFeO_3$ under illumination and results in enhanced cathodic photocurrents. To achieve a high amount of biocatalysts in front of the electrode, the enzyme has been embedded into polyethylenimine and stabilized via crosslinking. SEM investigations reveal a rather high surface roughness with a height of about 1.1 μm (Figure S7). Here, a GOx activity of at least 0.8 ± 0.09 U has been integrated into this polymeric network (for details see Figure S8). The final $BiFeO_3$ | GOx electrode has been studied with respect to H_2O_2 sensitivity. It provides a similar signal response to a defined H_2O_2 concentration as an unmodified electrode, indicating that the enzyme modification does not affect the catalytic electrode activity (Figure S9). Furthermore, the $BiFeO_3$ | GOx electrodes have been investigated via chopped light voltammetry in the absence and presence of glucose. As depicted in Figure 2, the cathodic photocurrent is enhanced over the whole potential range after addition of 10 mM glucose ($\Delta I = 14.6 \pm 2.8\ \mu A\,cm^{-2}$, 0 mV vs. Ag/AgCl (1 M KCl)), while electrodes without GOx show no signal increase (Figure S10). This clearly confirms the functionality of the constructed signal chain as illustrated in Scheme 1.

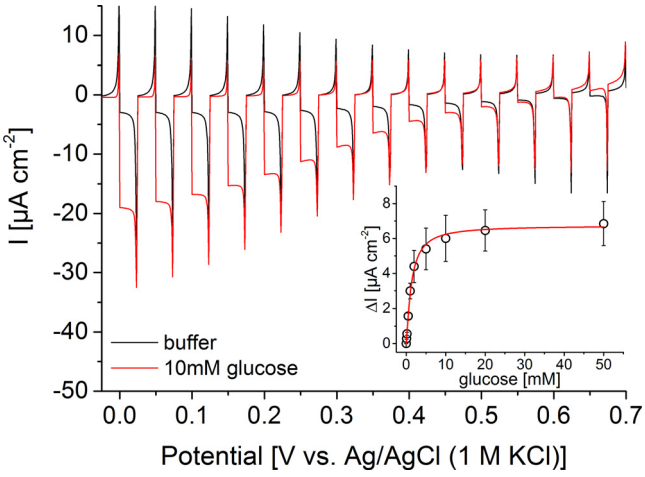

Figure 2. Chopped-light voltammetry of a $BiFeO_3$ | GOx electrode in the presence and absence of 10 mM glucose (100 $mW\,cm^{-2}$; potential vs. Ag/AgCl, 1 M KCl; 10 $mV\,s^{-1}$). Inset: photocurrent density change ΔI of a $BiFeO_3$ | GOx electrode before and after addition of different glucose concentrations (100 $mW\,cm^{-2}$; 0.2 V vs. Ag/AgCl, 1 M KCl).

The maximum current of the $BiFeO_3$ | GOx electrode under glucose-saturated conditions corresponds to a H_2O_2 concentration of about 300 μM produced by the immobilized GOx. This concentration is comparable to the oxygen content in solution and suggests that the electrode performance is mainly restricted by the low oxygen availability in solution. This is a typical problem of oxygen-reducing electrodes, but can be circumvented by improving the oxygen transport to the electrode.[32]

The onset potential has been determined to be 0.602 ± 0.007 V vs. Ag/AgCl (1 M KCl), which demonstrates the efficient coupling of enzymatic H_2O_2 production and light-triggered turnover. The concentration dependency of the $BiFeO_3$ | GOx electrodes has been determined at a bias of 0.2 V vs. Ag/AgCl by successively increasing the glucose concentration (Figure 2). Here, a signal response has been observed starting at 100 μM glucose and leveling off at about 50 mM. An apparent K_M value of 1.3 ± 0.1 mM can be determined. The results illustrate the good conditions found for the construction of the photobiocathode. Glucose conversion can be combined with current generation at rather positive potential.

Subsequently, the photobiocathode is coupled to an inverse opal (IO)-TiO_2 photobioanode modified with PbS quantum dots (QDs), redox polymer (P_{Os}) and FAD glucose dehydrogenase (FAD-GDH) as reported by us before (for a SEM image see Figure S11).[14] While PbS QDs act as photoactive entity and introduce visible light sensitivity into the photoanode, the redox polymer mediates the electron transfer from the enzyme towards the QDs to the IO-TiO_2 architecture in the presence of glucose under illumination as depicted in Scheme 1. The photobioanode gives rise to maximum anodic photocurrents of $151 \pm 29\ \mu A\,cm^{-2}$ at 0 V vs. Ag/AgCl (1 M KCl) in the presence of glucose (Figure 3A). An open circuit potential of -0.463 ± 0.004 V vs. Ag/AgCl (1 M KCl) is formed under illumination, allowing electron extraction from biocatalytic glucose oxidation at

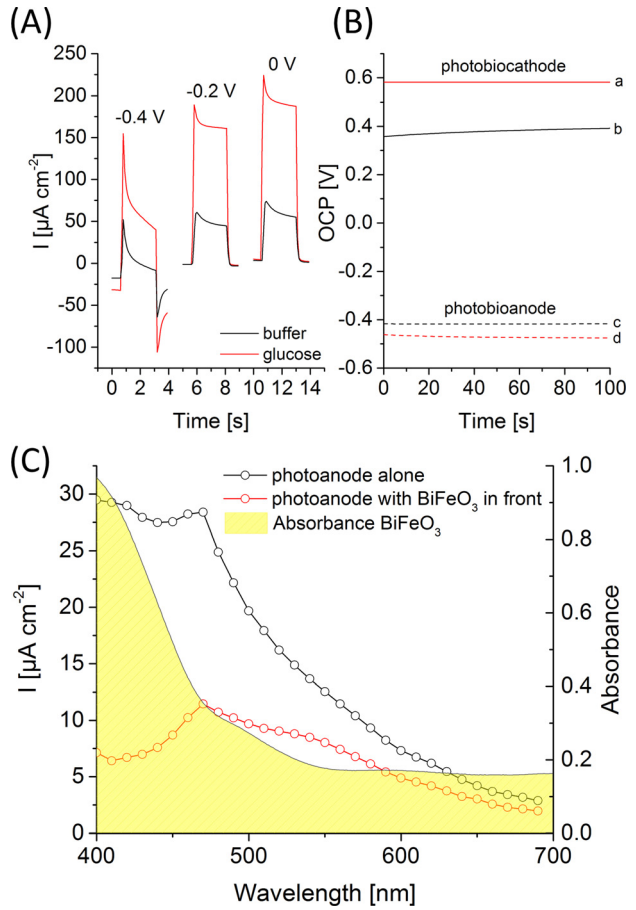

Figure 3. A) Photocurrent response of an IO-TiO_2 | PbS | P_{Os} | FAD-GDH electrode in the presence and absence of 100 mM glucose at different potentials (100 mW cm^{-2}; potential vs. Ag/AgCl, 1 M KCl). B) Potentiometric measurement of the photobiocathode (a,b) and the photobioanode (c,d) in the presence (a,d) and absence (b,c) of glucose under illumination (100 mW cm^{-2}; OCP vs. Ag/AgCl, 1 M KCl). C) Wavelength-dependent photocurrent of an IO-TiO_2 | PbS | P_{Os} | FAD-GDH electrode with unimpeded illumination (black curve) and by illumination through the $BiFeO_3$ (red curve) material (0 V vs. Ag/AgCl, 1 M KCl). Additionally, the UV/Vis spectrum of $BiFeO_3$ is shown.

quite negative bias (Figure 3B). We have chosen PbS as photoactive entity due to its small band gap,[14] this should allow excitation at higher wavelengths as compared to the $BiFeO_3$ material.

To scrutinize the influence of the $BiFeO_3$ absorbance on the signal generation at the photobioanode, wavelength resolved measurements are performed with and without $BiFeO_3$ in front of the electrode (Figure 3C). As expected, the photoresponse of the photobioanode is diminished, particularly at wavelengths below 550 nm where $BiFeO_3$ is absorbing. But even under these conditions, a reasonable part of the light can pass the cathode for the excitation of the photobioanode, resulting in pronounced photocurrents of $83.5 \pm 15.2\ \mu A\,cm^{-2}$ under white light illumination (Figure S12). Since this is still larger than the photocurrent generation at the photobiocathode, advantageous conditions are provided for an on top arrangement of both electrodes (Figure S13). Thus, the optical properties of the photobiocathode nicely fit to the excitation range of the photobioanode, so that both can be simultaneously excited.

Consequently, for the construction of the PBTC, the $BiFeO_3$ | GOx electrode and the IO-TiO_2 | PbS | P_{Os} | FAD-GDH electrode have been arranged opposite each other so that the light passes the photobiocathode first and then reaches the photobioanode (Scheme 1). The advantage of this arrangement is that the necessary space for the cell is reduced and this allows a higher energy yield per area (or volume). *I–V* curves have been performed in the presence and absence of glucose under illumination in order to investigate the power generation of the cell. As illustrated in Figure 4, a quite large open cell voltage (OCV) of 0.995 ± 0.006 V and a photocurrent of up to $23.9 \pm 3.5\ \mu A\,cm^{-2}$ has been obtained with glucose in solution. A maximum power density of $8.1 \pm 1.1\ \mu W\,cm^{-2}$ can be determined at a cell potential of 0.55 ± 0.02 V. The OCV correlates well with the individual potentials of the photobiocathode and photobioanode (Figure 3B) under illumination, while the photocurrent of the cell is limited by the cathodic reaction. In the absence of glucose only small photocurrents of $1.8 \pm 0.65\ \mu A\,cm^{-2}$ are observed. This clearly demonstrates that the biocatalytic glucose turnover is necessary to drive both, the photobiocathode and the photobioanode. The PBTC shows acceptable stability with glucose in solution and under illumination with high intensity reaching 70% of the initial signal after 20 min operation (Figure S14). To the best of our knowledge, the results represent the first example for a PBTC, in which the power generation is realized by combination of two photobioelectrodes that can be arranged sandwich-like saving space. While the photocurrent amplitude is currently modest, the open circuit voltage is higher as compared to classical light-insensitive glucose biofuel cells.[33–37] However, since inorganic metal oxide and quantum dot-based photoelectrodes already allow currents in the mA range,[38,39] there

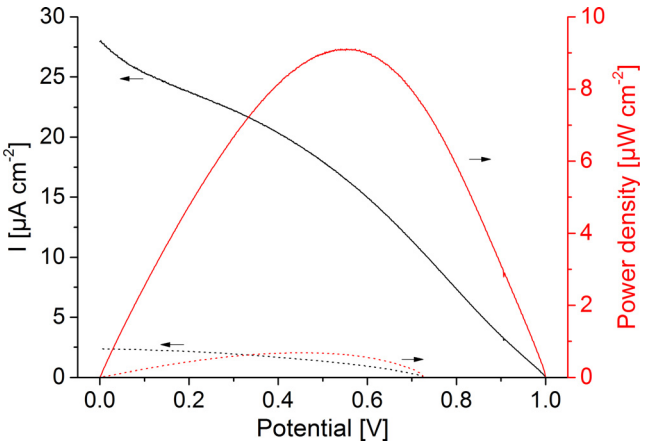

Figure 4. Current and power density of the photobioelectrochemical tandem cell, consisting of an $BiFeO_3$ | GOx photobiocathode and an IO-TiO_2 | PbS | P_{Os} | FAD-GDH photobioanode in the presence (solid lines) and absence (dotted lines) of 100 mM glucose and under illumination. The tandem cell is arranged in a sandwich-like manner, so that the photoexcitation of both electrodes is realized by lighting through the semi-transparent photobiocathode (100 mW cm^{-2}; 5 mV s^{-1}).

is great potential for improvement for future biohybrid tandem solar cells, if the biotic/abiotic interface is adjusted.

In summary, we have demonstrated a proof-of-concept for a photobioelectrochemical tandem cell in which two photoelectrodes are functionally coupled with two biocatalysts for supplying a light-driven reaction with charge carriers from glucose conversion. A $BiFeO_3$ | GOx electrode has been designed for the cathodic reaction, which is based on a high photoelectrocatalytic activity towards H_2O_2 and enzymatic H_2O_2 production in the presence of glucose, thereby giving access to first photocurrents at quite positive potentials of about 0.6 V vs. Ag/AgCl. The photobiocathode has been combined with a glucose-converting IO-TiO_2 | PbS | P_{Os} photoanode hosting FAD-GDH in a sandwich-like arrangement so that a reasonable photoexcitation of both photoactive electrodes is realized by illumination through the semitransparent photobiocathode. The biohybrid cell is capable of generating electricity under illumination and in the presence of one fuel molecule, reaching a high OCV of about 1 V. It is anticipated that this study will advance the development of biohybrid tandem cells for energy demands so that improvements in the photoelectrode construction and enzyme/semiconductor interface (e.g. by nanostructuring) will give access to more efficient systems with higher power output in future.

Acknowledgements

The authors are thankful to the BMBF Germany (Biotechnology 2020+, projects: 031B0557A + B), which has partially supported this research. A.R. and W.S. are grateful for financial support by the Deutsche Forschungsgemeinschaft (DFG, German Research Foundation) under Germany's Excellence Strategy—EXC 2033–390677874—RESOLV. Open access funding enabled and organized by Projekt DEAL.

Conflict of interest

The authors declare no conflict of interest.

Keywords: biocatalysis · biofuel cells · energy harvesting · photocatalysis · photoelectrochemistry

[1] N. Kornienko, J. Z. Zhang, K. K. Sakimoto, P. Yang, E. Reisner, *Nat. Nanotechnol.* **2018**, *13*, 890 – 899.
[2] A. Ruff, F. Conzuelo, W. Schuhmann, *Nat. Catal.* **2020**, *3*, 214 – 224.
[3] S. H. Lee, D. S. Choi, S. K. Kuk, C. B. Park, *Angew. Chem. Int. Ed.* **2018**, *57*, 7958 – 7985; *Angew. Chem.* **2018**, *130*, 8086 – 8116.
[4] V. Pardo-Yissar, E. Katz, J. Wasserman, I. Willner, *J. Am. Chem. Soc.* **2003**, *125*, 622 – 623.
[5] R. K. Yadav, G. H. Oh, N.-J. Park, A. Kumar, K. Kong, J.-O. Baeg, *J. Am. Chem. Soc.* **2014**, *136*, 16728 – 16731.
[6] S. K. Kuk, R. K. Singh, D. H. Nam, R. Singh, J.-K. Lee, C. B. Park, *Angew. Chem. Int. Ed.* **2017**, *56*, 3827 – 3832; *Angew. Chem.* **2017**, *129*, 3885 – 3890.
[7] S. Zhao, J. Völkner, M. Riedel, G. Witte, Z. Yue, F. Lisdat, W. J. Parak, *ACS Appl. Mater. Interfaces* **2019**, *11*, 21830 – 21839.
[8] A. Efrati, C.-H. Lu, D. Michaeli, R. Nechushtai, S. Alsaoub, W. Schuhmann, I. Willner, *Nat. Energy* **2016**, *1*, 15021.
[9] M. Riedel, N. Sabir, F. W. Scheller, W. J. Parak, F. Lisdat, *Nanoscale* **2017**, *9*, 2814 – 2823.
[10] Z. Li, W. Wang, C. Ding, Z. Wang, S. Liao, C. Li, *Energy Environ. Sci.* **2017**, *10*, 765 – 771.
[11] M. Riedel, A. Ruff, W. Schuhmann, F. Lisdat, F. Conzuelo, *Chem. Commun.* **2020**, *56*, 5147 – 5150.
[12] M. Riedel, F. Lisdat, *ACS Appl. Mater. Interfaces* **2018**, *10*, 267 – 277.
[13] C.-Y. Lee, H. S. Park, J. C. Fontecilla-Camps, E. Reisner, *Angew. Chem. Int. Ed.* **2016**, *55*, 5971 – 5974; *Angew. Chem.* **2016**, *128*, 6075 – 6078.
[14] M. Riedel, W. J. Parak, A. Ruff, W. Schuhmann, F. Lisdat, *ACS Catal.* **2018**, *8*, 5212 – 5220.
[15] K. P. Sokol, W. E. Robinson, J. Warnan, N. Kornienko, M. M. Nowaczyk, A. Ruff, J. Z. Zhang, E. Reisner, *Nat. Energy* **2018**, *3*, 944.
[16] K. P. Sokol, W. E. Robinson, A. R. Oliveira, J. Warnan, M. M. Nowaczyk, A. Ruff, I. A. C. Pereira, E. Reisner, *J. Am. Chem. Soc.* **2018**, *140*, 16418 – 16422.
[17] M. Riedel, J. Wersig, A. Ruff, W. Schuhmann, A. Zouni, F. Lisdat, *Angew. Chem. Int. Ed.* **2019**, *58*, 801 – 805; *Angew. Chem.* **2019**, *131*, 811 – 815.
[18] K. R. Stieger, S. C. Feifel, H. Lokstein, M. Hejazi, A. Zouni, F. Lisdat, *J. Mater. Chem. A* **2016**, *4*, 17009 – 17017.
[19] D. S. Choi, Y. Ni, E. Fernández-Fueyo, M. Lee, F. Hollmann, C. B. Park, *ACS Catal.* **2017**, *7*, 1563 – 1567.
[20] W. Jia, S. Schwamborn, C. Jin, W. Xia, M. Muhler, W. Schuhmann, L. Stoica, *Phys. Chem. Chem. Phys.* **2010**, *12*, 10088 – 10092.
[21] K. Elouarzaki, M. Bourourou, M. Holzinger, A. L. Goff, R. S. Marks, S. Cosnier, *Energy Environ. Sci.* **2015**, *8*, 2069 – 2074.
[22] B. Reuillard, K. H. Ly, P. Hildebrandt, L. J. C. Jeuken, J. N. Butt, E. Reisner, *J. Am. Chem. Soc.* **2017**, *139*, 3324 – 3327.
[23] J. Zhang, L. Tu, S. Zhao, G. Liu, Y. Wang, Y. Wang, Z. Yue, *Biosens. Bioelectron.* **2015**, *67*, 296 – 302.
[24] S. P. Berglund, F. F. Abdi, P. Bogdanoff, A. Chemseddine, D. Friedrich, R. van de Krol, *Chem. Mater.* **2016**, *28*, 4231 – 4242.
[25] T. Ameri, N. Li, C. J. Brabec, *Energy Environ. Sci.* **2013**, *6*, 2390 – 2413.
[26] J.-T. Han, Y.-H. Huang, X.-J. Wu, C.-L. Wu, W. Wei, B. Peng, W. Huang, J. B. Goodenough, *Adv. Mater.* **2006**, *18*, 2145 – 2148.
[27] P. Yilmaz, D. Yeo, H. Chang, L. Loh, S. Dunn, *Nanotechnology* **2016**, *27*, 345402.
[28] J. Tauc, R. Grigorovici, A. Vancu, *Phys. Status Solidi B* **1966**, *15*, 627 – 637.
[29] J. F. Ihlefeld, N. J. Podraza, Z. K. Liu, R. C. Rai, X. Xu, T. Heeg, Y. B. Chen, J. Li, R. W. Collins, J. L. Musfeldt, et al., *Appl. Phys. Lett.* **2008**, *92*, 142908.
[30] G. Wohlfahrt, S. Witt, J. Hendle, D. Schomburg, H. M. Kalisz, H.-J. Hecht, *Acta Crystallogr. Sect. D* **1999**, *55*, 969 – 977.
[31] H. Yoshida, G. Sakai, K. Mori, K. Kojima, S. Kamitori, K. Sode, *Sci. Rep.* **2015**, *5*, 13498.
[32] N. Mano, A. de Poulpiquet, *Chem. Rev.* **2018**, *118*, 2392 – 2468.
[33] H. Sakai, T. Nakagawa, Y. Tokita, T. Hatazawa, T. Ikeda, S. Tsujimura, K. Kano, *Energy Environ. Sci.* **2009**, *2*, 133 – 138.
[34] C. Agnès, B. Reuillard, A. Le Goff, M. Holzinger, S. Cosnier, *Electrochem. Commun.* **2013**, *34*, 105 – 108.
[35] V. Scherbahn, M. T. Putze, B. Dietzel, T. Heinlein, J. J. Schneider, F. Lisdat, *Biosens. Bioelectron.* **2014**, *61*, 631 – 638.
[36] R. D. Milton, D. P. Hickey, S. Abdellaoui, K. Lim, F. Wu, B. Tan, S. D. Minteer, *Chem. Sci.* **2015**, *6*, 4867 – 4875.
[37] A. J. Gross, X. Chen, F. Giroud, C. Abreu, A. Le Goff, M. Holzinger, S. Cosnier, *ACS Catal.* **2017**, *7*, 4408 – 4416.

[38] S. Rühle, A. Y. Anderson, H.-N. Barad, B. Kupfer, Y. Bouhadana, E. Rosh-Hodesh, A. Zaban, *J. Phys. Chem. Lett.* **2012**, *3*, 3755 – 3764.

[39] G. H. Carey, A. L. Abdelhady, Z. Ning, S. M. Thon, O. M. Bakr, E. H. Sargent, *Chem. Rev.* **2015**, *115*, 12732 – 12763.

Manuscript received: September 4, 2020
Accepted manuscript online: October 2, 2020
Version of record online: November 24, 2020

